VIROLOGY

Crystal structure of bovine herpesvirus 1 glycoprotein D bound to nectin-1 reveals the basis for its low-affinity binding to the receptor

Dan Yue[1], Zhujun Chen[1], Fanli Yang[1], Fei Ye[1], Sheng Lin[1], Bin He[1], Yanwei Cheng[1,2], Jichao Wang[1], Zimin Chen[1], Xi Lin[1], Jing Yang[1], Hua Chen[1], Zhonglin Zhang[1], Yu You[1], Honglu Sun[1], Ao Wen[1], Lingling Wang[1], Yue Zheng[1], Yu Cao[1,3], Yuhua Li[1,4]*, Guangwen Lu[1]*

Bovine herpesvirus 1 (BHV-1) has received increasing attention for its potential oncolytic applications. BHV-1 recognizes nectin-1 for cell entry via viral glycoprotein D (gD) but represents a low-affinity nectin-1 binding virus. The molecular basis underlying this low receptor-binding affinity, however, remains unknown. Here, the crystal structures of BHV-1 gD in the free and nectin-1–bound forms are presented. While showing an overall resembled nectin-1 binding mode to other alphaherpesvirus gDs, BHV-1 gD has a unique G-strand/α2-helix interloop that disturbs gD/nectin-1 interactions. Residue R188 residing in this loop is observed to otherwise cause strong steric hindrance with the bound receptor, making a large conformational change of the loop a prerequisite for nectin-1 engagement. Subsequently, substitution of R188 with glycine markedly enhances the affinity of the BHV-1-gD/nectin-1 interaction (by about fivefold). These structural and functional data delineate the receptor-recognition basis for BHV-1, which might facilitate BHV-1–based oncolytic design in the future.

INTRODUCTION

Bovine herpesvirus 1 (BHV-1) is an important agricultural pathogen worldwide (*1*). It can cause acute infections in cattle, leading to severe diseases such as infectious rhinotracheitis, pustular vulvovaginitis, conjunctivitis, and abortions (*1*). In addition, the virus can establish latency in sensory neurons, posing a lifelong risk of reactivation of viral infections (*1*). Despite the economic threat of BHV-1 to the livestock industry, the virus has recently drawn increasing attention for its potential oncolytic applications. As a species-specific virus with a restricted host range, BHV-1 is unable to productively infect normal human cells (*2*). Nevertheless, the virus can efficiently target immortalized and transformed human cells, making it an attractive oncolytic candidate for cancer therapy (*2*). As a wild-type oncolytic virus, BHV-1 has a notable advantage when compared with other oncolytic viruses exemplified by the herpes simplex virus (HSV), because the virus can be used potentially for oncolysis without any genetic modification (*3*). Furthermore, accumulating evidence shows that BHV-1 is a promising broad-spectrum oncolytic vector that can infect and kill human tumor cells from a variety of histological origins (*4*).

BHV-1 is a large enveloped double-stranded DNA virus that belongs to the *Varicellovirus* genus in the *Alphaherpesvirinae* subfamily (*1*). Alphaherpesviruses encode a large number of envelope glycoproteins to mediate both receptor binding and fusion between the viral envelope and cell membrane, thereby initiating the entry of viral particles into host cells (*5*). Of these, at least four glycoproteins (glycoprotein B, D, H, and L or gB, gD, gH, and gL) are essential (*6*). Notably, the virus gD is a canonical viral ligand of alphaherpesvirus entry receptors, and successful entry of the virus into cells depends on the binding of gD to the cell surface receptor(s) (*7*).

To date, multiple receptors targeted by gD have been identified. These include the 3-O-sulfated-heparan sulfate (*8*), herpes virus entry mediator (also called HveA) (*9*), nectin-1 (also called HveC and poliovirus receptor–related protein 1) (*10*), nectin-2 (HveB) (*11*), and HveD (PVR, CD155) (*10*). Of these receptors, nectin-1 serves as a universal entry receptor for multiple alphaherpesviruses, including HSV-1 and HSV-2, pseudorabies virus (PRV), and BHV-1 (*12*). Nectin-1 is a Ca^{2+}-independent immunoglobulin (Ig)–like cell adhesion molecule of the nectin and nectin-like family (*13*). Through homophilic and/or heterophilic dimerization, nectin-1 plays important roles in cellular activities such as cell adhesion, polarization, movement, and proliferation (*14*). In addition, expression of nectin-1 is potentially associated with poor prognosis in several tumor types (*15*, *16*). Topologically, nectin-1 is a single-pass type I membrane glycoprotein that consists of an extracellular region with three Ig-like domains (one terminal IgV domain followed by two consecutive IgC domains), a transmembrane region, and a cytoplasmic domain containing the afadin-binding motif (*17*). The IgV domain of nectin-1 is responsible for both receptor dimerization and gD engagement (*18*). Previous studies have already delineated the nectin-1 binding basis, via high-resolution structures, for HSV-1, HSV-2, and PRV gDs (*19*–*21*). These structures reveal that gD consists of an IgV-like core and long N- and C-terminal extensions. The gD/nectin-1 interaction is mediated mainly by the terminal extension elements in gD and the membrane-distal IgV domain of the receptor (*19*, *21*, *22*). In comparison to these structurally characterized alphaherpesviral gDs, BHV-1 gD shares very limited sequence identity (~23% to HSV-1 gD, ~23% to HSV-2 gD, and ~33% to PRV gD). Although these gDs inhibit the entry of both homologous and heterologous viruses (*23*), which points to an analogous nectin-1 binding mode, BHV-1 gD is unique in light of the previous report showing that the gD from BHV-1 displays lower nectin-1 binding affinity when compared with that of homologous gDs (*12*). The molecular basis underlying this low-affinity binding, however, remains unknown. As an important agricultural pathogen

[1]West China Hospital Emergency Department (WCHED), State Key Laboratory of Biotherapy, West China Hospital, Sichuan University, and Collaborative Innovation Center of Biotherapy, Chengdu, Sichuan 610041, China. [2]Department of Emergency, Henan Provincial People's Hospital, People's Hospital of Zhengzhou University, People's Hospital of Henan University, Zhengzhou, Henan, 450003, China. [3]Disaster Medicine Center, Sichuan University, Chengdu, Sichuan 610041, China. [4]Department of Arbovirus Vaccine, National Institutes for Food and Drug Control, Beijing, 102629, China.
*Corresponding author. Email: liyuhua@nifdc.org.cn (Y.L.); lugw@scu.edu.cn (G.L.)

and a critical avenue for cancer therapy, studying structural features of the viral gD from BHV-1 and the gD/nectin-1 complex should provide valuable information. Moreover, nectin-1 expression and the subsequent gD/nectin-1 interaction are associated with HSV-1 oncolytic sensitivity (*24*). Thus, the detailed atomic structure(s) will contribute to rational design of therapeutic agents for treating tumors based on BHV-1.

In this study, we first showed that BHV-1 gD interacts with human and bovine nectin-1 (HU-nectin-1 and BO-nectin-1) with comparable binding affinities. This observed affinity, however, was more than 20-fold lower than those observed for HSV and PRV gDs. The atomic structures of BHV-1 gD in the free form and in the receptor-bound form with BO-nectin-1 were solved at 2.5 and 2.2 Å, respectively. BHV-1 gD presented a similar overall protein fold and a homologous nectin-1 binding mode when compared with other alphaherpesviral gDs. The structures, however, revealed a large conformational change in the intervening loop connecting the G-strand and the α2-helix before and after receptor binding, which has not been observed in other structurally characterized gDs. A loop-residing arginine (R188) causes strong steric hindrance that hampers receptor interaction, thus explaining the observed conformational change to enable nectin-1 binding. We further showed that substitution of R188 with glycine enhanced the BHV-1-gD/nectin-1 binding by about fivefold.

RESULTS

BHV-1 gD engages nectin-1 with lower affinity than other alphaherpesviral gDs

BHV-1 gD similarly recognizes nectin-1 as the cellular receptor but binds with lower affinity than HSV and PRV gDs (*12*). Therefore, we carried out the real-time binding kinetic study between the viral protein and the receptor in solution. BHV-1 gD, with a type I transmembrane topology, contains a large ectodomain spanning amino acids 1 to 342 (residue numbering is based on the mature protein to facilitate sequence comparison with other structurally characterized gDs) (Fig. 1A). This ectodomain of BHV-1 gD (hereafter referred to as gD342) was prepared (Fig. 1B), and its interaction with the IgV domain of BO- and HU-nectin-1 was measured by surface plasmon resonance (SPR) (Fig. 1C). As expected, potent interactions between gD342 and BO- or HU-nectin-1 were observed. The recorded kinetic data showed a slow-on but fast-off binding mode, which is in agreement with a previous study reporting similar slow association with fast dissociation binding curves between the ectodomain protein of BHV-1 gD (an equivalent to gD342) and HU-nectin-1 (*12*). Because no fitting algorithms are currently available for calculations of the slow-on/fast-off kinetic data, the accurate dissociation constant (K_D) values for gD342 binding to BO- and HU-nectin-1 were not determined.

Inspired by the observation that the membrane-proximal region of the gD ectodomain can interfere with nectin-1 binding (*25*), we further constructed two gD variants with ectodomain residues 1 to 301 (referred to as gD301) and 1 to 274 (referred to as gD274) (Fig. 1A). The resultant proteins were individually prepared to homogeneity (Fig. 1B) and tested for their real-time interactions with BO- and HU-nectin-1 via SPR (Fig. 1, D and E). Both gD301 and gD274 showed, unlike gD342, fast-on/fast-off kinetics toward nectin-1 (Fig. 1, D and E). These kinetic data were used to calculate affinities using the steady-state affinity model. The determined K_D values were 340.6 ± 106.1 nM, 879.2 ± 100.8 nM, 498.7 ± 156.5 nM, and 700.8 ± 67.6 nM for the gD301/BO-nectin-1, gD301/HU-nectin-1, gD274/BO-nectin-1, and gD274/HU-nectin-1, respectively (Table 1). The results demonstrated that BHV-1 gD (whole ectodomain or truncated) was capable of

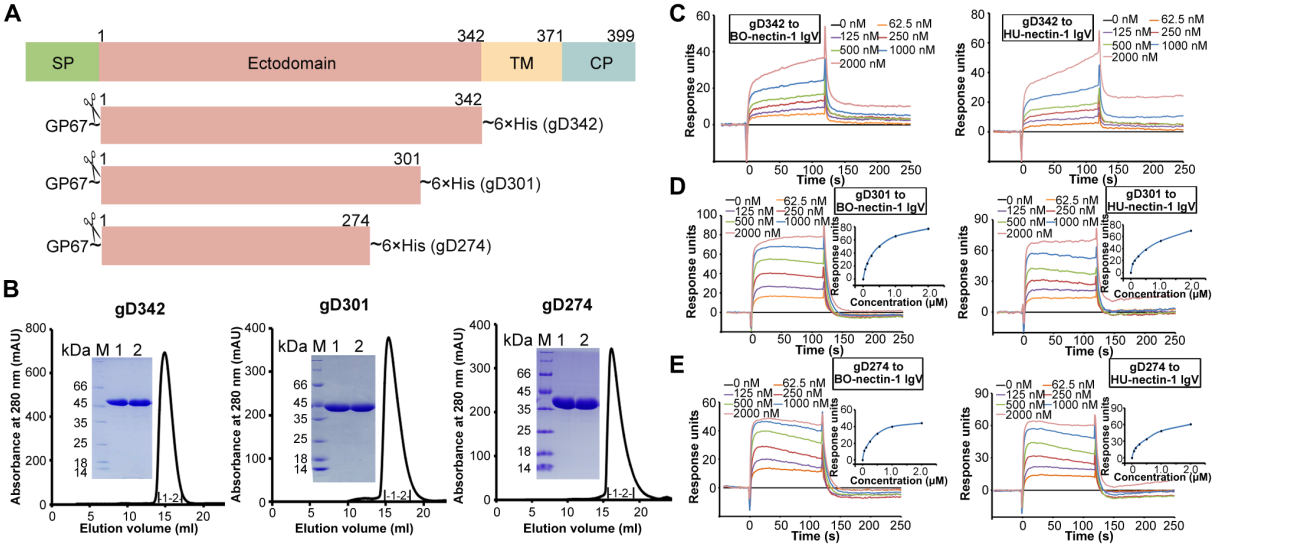

Fig. 1. BHV-1 gD engages nectin-1 with low binding affinities. (**A**) A schematic view of BHV-1 gD. The signal peptide (SP), ectodomain, transmembrane domain (TM), and cytoplasmic domain (CP) were marked with the boundary residue numbers. For recombinant expression of BHV-1 gD in insect cells, the protein was truncated (amino acids 1 to 342 for gD342, amino acids 1 to 301 for gD301, and amino acids 1 to 274 for gD274), engineered with a GP67 signal peptide for secretion, and added with a C-terminal 6×His tag for purification. (**B**) Representative size-exclusion chromatographs of gD342, gD301, and gD274. The separation chromatograph of the protein and the SDS–polyacrylamide gel electrophoresis analyses of the pooled samples were shown. Lane 1: The pooled sample collected from the first half of the protein elution peak. Lane 2: Sample collected from the second half of the peak. (**C** to **E**) An SPR assay characterizing the binding kinetics between BHV-1 gD and nectin-1 IgV. Gradient concentrations of BO- or HU-nectin-1 IgV were flowed through gD342, gD301, and gD274 immobilized on the chip surface. The real-time binding profiles are recorded and shown.

Table 1. Statistics of the kinetic binding affinities between BHV-1 gD and nectin-1 IgV determined by SPR. The fast-on/fast-off kinetic data are analyzed by the steady-state affinity model. The results from three independent experiments are listed.

Binding pair	K_D (M)	Average K_D (M)	SD for K_D	Model
gD274 to HU-nectin-1-IgV	7.575×10^{-7}	7.008×10^{-7}	0.676×10^{-7}	Steady-state affinity
	6.260×10^{-7}			
	7.188×10^{-7}			
gD274 to BO-nectin-1-IgV	6.752×10^{-7}	4.987×10^{-7}	1.565×10^{-7}	Steady-state affinity
	4.437×10^{-7}			
	3.771×10^{-7}			
gD301 to HU-nectin-1-IgV	7.648×10^{-7}	8.792×10^{-7}	1.008×10^{-7}	Steady-state affinity
	9.183×10^{-7}			
	9.546×10^{-7}			
gD301 to BO-nectin-1-IgV	2.591×10^{-7}	3.406×10^{-7}	1.061×10^{-7}	Steady-state affinity
	3.022×10^{-7}			
	4.606×10^{-7}			
gD301-R188G to BO-nectin-1-IgV	7.908×10^{-8}	7.054×10^{-8}	1.352×10^{-8}	Steady-state affinity
	5.495×10^{-8}			
	7.758×10^{-8}			
gD301-Y190G to BO-nectin-1-IgV	8.067×10^{-7}	7.502×10^{-7}	1.648×10^{-7}	Steady-state affinity
	8.974×10^{-7}			
	5.646×10^{-7}			

interacting with both the bovine and the human receptors, although the affinities for the former were slightly higher.

Note that the gDs lacking the membrane-proximal region from HSV (HSV-1 gD285) (*22*) and PRV (PRV gD284) (*19*) bind nectin-1 with about 17.1 and 18.4 nM affinities, respectively. The determined K_D values for BHV-1 gD represent more than 20-fold lower affinity for receptor binding.

Crystal structure of the free BHV-1 gD

As a step toward understanding the molecular basis underlying its lower affinity toward nectin-1, we first focused our attention on obtaining the BHV-1 gD structure in the free form. gD342, gD301, and gD274 were all subjected to intensive crystallization screenings, and a dataset of 2.5-Å resolution was lastly collected from the gD301 crystals. The solved structure, which was refined to R_{work} = 0.2071 and R_{free} = 0.2523 (table S1), contained three gD molecules within the crystallographic asymmetric unit. These three molecules were essentially the same structure, showing root mean square deviations of 0.278 to 0.619 Å for all the equivalent Cα pairs. Each molecule in the asymmetric unit adopted a structure composed of a center IgV-like core and long peripheral N- and C-terminal extensions (Fig. 2A).

The core IgV-like domain spanned residues E47 to S173. These amino acids assembled into a compact nine-stranded antiparallel (A′, B, C, C′, C″, D, E, F, and G) β barrel. In addition, two α helices (α1 and α1′) were also part of the core domain, topologically located between β strands B and C and C″ and D, respectively (Fig. 2, A and F). As observed in other known gD structures, BHV-1 gD also had a two-half kinked C″ strand connected via a distorted loop (Fig. 2, A and F). An intradomain disulfide bond formed between residues C108 and C117 and further stabilized the core structure (Fig. 2, A and F).

Surrounding the IgV-like core were two peripheral extension elements constituted by gD N-terminal residues P6 to V46 and gD C-terminal residues L174 to P248. The N-terminal extension folded to form a long loop embracing a little β strand (str2). This extension wrapped around the IgV-like core and the C-terminal α3 helix like a rope, with more than three-quarters of the overall globular-shaped gD enveloped by this extension. In addition, str2 further aligned in a parallel manner with the first half of strand C″ (Fig. 2A). The C-terminal extension adopted a more complex structure, composed of three α helices (α2, α3, and α3′), one β strand (str3), and several long intervening loops. These C-terminal elements extended over the core domain extensively, such that the α3 helix was sandwiched between the N-terminal loop and the IgV-like core and that the small str3 strand was positioned alongside the second half of the C″ strand in an antiparallel manner (Fig. 2A). Furthermore, amino acids C179 and C195 in the C-terminal extension were observed to form disulfide linkages with core residues C57 and C96, respectively, further tethering the terminal elements to the IgV-like core (Fig. 2, A and F).

As expected, the solved BHV-1 gD structure resembled those of HSV-1, HSV-2, and PRV gDs. Superimposition of these structures revealed overall well-aligned IgV-like core and terminal extension elements. Detailed structural comparison, however, revealed several differences in their compositions and locations for secondary structure elements (Fig. 2, B to E). For instance, both BHV-1 and PRV gDs had an α1′ helix located between strands C″ and D in the IgV-like core and an α3′ helix between the α2 helix and strand str3 in the C-terminal extension. These two helices, however, are not present in HSV-1 and HSV-2 gDs. Conversely, located between the core helix α1 and strand C, the HSV gDs contain an α1′ helix that is not present in either the BHV-1 or the PRV gD structures (Fig. 2, C to E).

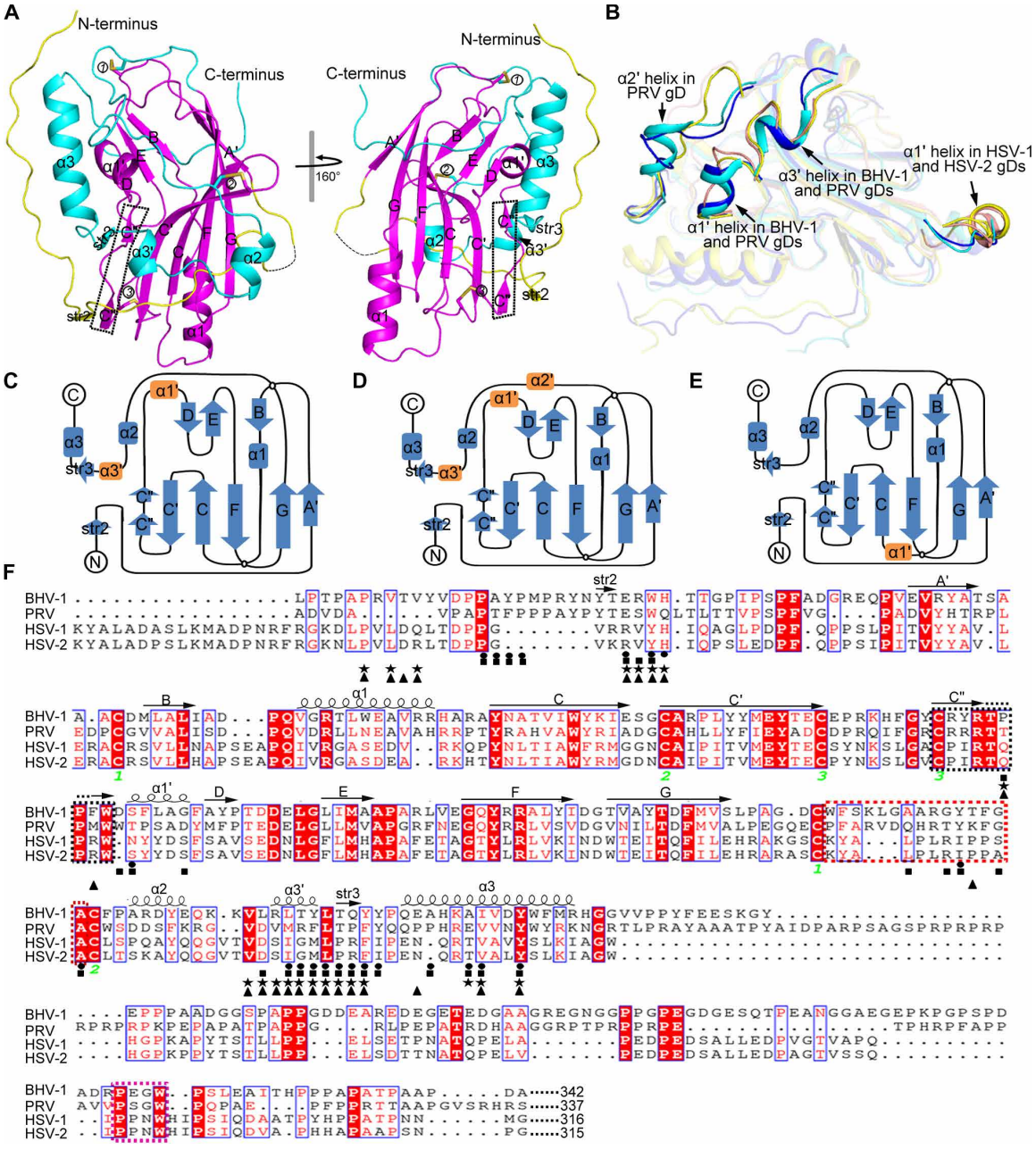

Fig. 2. Structure of free BHV-1 gD. (**A**) Cartoon representation of the overall structure. The extracellular domain of BHV-1 gD includes an IgV-like core (magenta) and N- and C-terminal extensions (yellow and cyan, respectively). The secondary structural elements and three disulfide bonds are labeled. (**B**) Comparison of HSV-1 (yellow), HSV-2 (salmon), PRV (cyan), and BHV-1 (blue) gD structures. The variant secondary structure elements are marked. (**C** to **E**) Topology diagrams of BHV-1 (C), PRV (D), and HSV-1 and HSV-2 (E) gDs. The figures are made on the basis of our BHV-1 gD structure, and the structures of PRV, HSV-1, and HSV-2 gDs with Protein Data Bank (PDB) codes of 5X5V, 1L2G, and 4MYW, respectively. The α helices and β strands are individually shown as rectangles and arrows, and those exhibiting differences are highlighted in orange. (**F**) Structure-based sequence alignment for BHV-1 gD and its homologs. The spirals and arrows indicate α helices and β strands, respectively. The cysteine residues forming disulfide bonds are marked numerically. The C″ strand, G/α2 interloop, and PxxW motif are highlighted with black, red, and magenta dotted rectangles, respectively. Residues of BHV-1, PRV, HSV-1, and HSV-2 gDs (*19*, *21*) interfacing with nectin-1 are marked with black circles, boxes, stars, and triangles, respectively.

Furthermore, BHV-1 gD lacks helix α2′ as with its HSV homologs, but the PRV protein has an extra helix (α2′) preceding the conserved α2 helix (Fig. 2, C to E).

Crystal structure of BHV-1 gD bound to BO-nectin-1 IgV

In light of our SPR observations showing that all BHV-1 gD constructs readily interacted with BO- and HU-nectin-1 with the two truncated forms exhibiting higher binding affinities, we subsequently prepared the ligand/receptor complex using gD301 for costructure studies. As expected, gD301 formed a stable complex with the IgV domain of both BO- and HU-nectin-1 (fig. S1). The gD in complex with the BO-nectin-1 receptor was lastly crystallized. The final structure was solved at 2.2-Å resolution with an R_{work} of 0.2144 and an R_{free} of 0.2463 (table S1) and contained two gD301/BO-nectin-1-IgV complexes in

the asymmetric unit. In each complex, one gD301 engaged a single receptor molecule (Fig. 3A), demonstrating a 1:1-binding mode as observed in other alphaherpesviral gDs (*19*–*22*).

For the viral ligand, it used mainly the terminal extension elements to interact with the receptor. These elements included helices α3 and α3′, strand str3, and the intervening loops connecting strand G with helix α2 and helices α3′ with α3 in the C-terminal extension and the flanking loops of the str2 strand in the N-terminal extension (Fig. 3A). Upon receptor binding, a total surface area of about 966.4 $Å^2$ was buried in these extension elements (table S2). For the nectin-1 receptor, it expectedly adopted a typical Ig-like V-set β barrel structure and used the slightly concave CC′C″ FG sheet to accommodate the viral ligand (Fig. 3A). The buried surface area in the nectin-1 receptor was calculated to be about 950.1 $Å^2$ (table S2).

In general, the engagement of the receptor did not induce notable structural changes in the part of BHV-1 gD301 that was solved in the complex structure. Superimposition of the free and nectin-1–bound gD structures, however, revealed apparent conformational differences in the N-terminal loop and in the loop linking helix α2 to strand G (hereafter referred to as the G/α2 interloop). After nectin-1 binding, the conformation of the N-terminal loop was observed to adjust slightly to accommodate the bound receptor, whereas the loop linking helix α2 to strand G, especially the middle part of the loop extending from G185 to T191, was reoriented, moving away from nectin-1 (Fig. 3B). Notably, these loop reorientations represent a prerequisite for nectin-1 recognition by BHV-1 gD, which would otherwise cause strong steric hindrance with the bound receptor (see also results below in "Arg^{188} is a critical residue determining the low-affinity interaction between BHV-1 gD and nectin-1" section).

As expected, the observed nectin-1 binding mode for BHV-1 gD resembled those of structurally characterized gDs from other alphaherpesviruses, including HSV-1, HSV-2, and PRV (*19*–*22*). In each case, the N- and C-terminal extensions of gD were used for nectin-1 recognition, engaging the same CC′C″ FG sheet in the receptor (Fig. 3, C to F). We further compared the total surface areas buried in the viral ligand and the receptor for these gD/nectin-1 pairs. Although slight

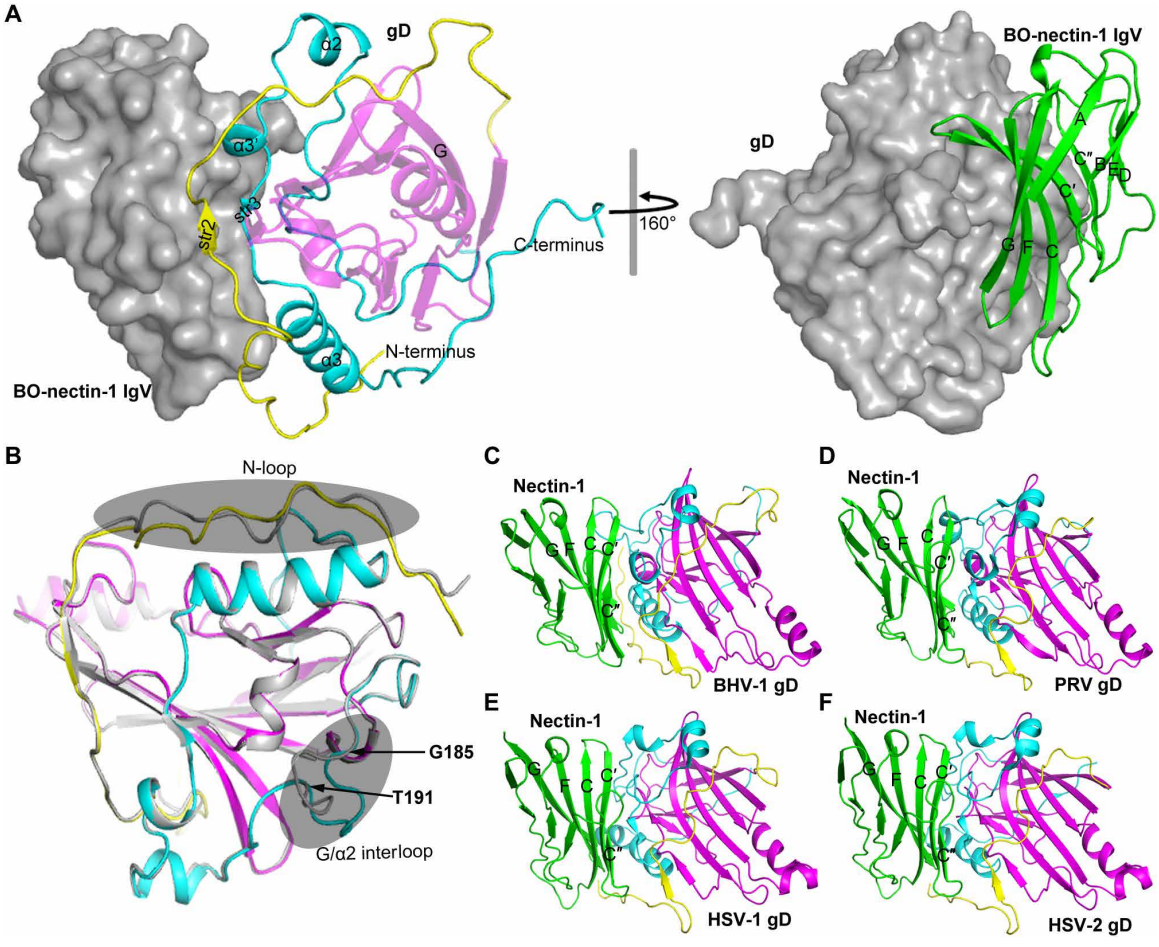

Fig. 3. Structure of BHV-1 gD bound to BO-nectin-1 IgV. (**A**) An overview of the complex structure. The IgV-like core and the N- and C-terminal extensions of BHV-1 gD and the nectin-1 receptor are colored magenta, yellow, cyan, and green, respectively. The left panel is rotated around a vertical axis for about 160° to generate the right one. BO-nectin-1 IgV in the left panel and gD in the right panel are shown in surface representation. (**B**) Structural comparison of the BHV-1 gD structures in the free (gray) and the nectin-1 bound form [colored as in (A)]. The N-terminal loop and the G/α2 interloop that experience conformational change upon receptor binding are shaded. (**C** to **F**) Homologous nectin-1 binding mode for alphaherpesviral gDs. (C) Structure of BHV-1 gD bound to BO-nectin-1. (D) Structure of PRV gD bound to swine nectin-1 (PDB code: 5X5W). (E) Structure of HSV-1 gD bound to HU-nectin-1 (PDB code: 3U82). (F) Structure of HSV-2 gD bound to HU-nectin-1 (PDB code: 4MYW). The complex structures are oriented similarly and aligned in parallel. The coloring scheme follows that in (A).

differences exist, the interface areas for these pairs were comparable and calculated to be about 1916.5, 1787.4, 1910.3, and 2289 Å^2 for BHV-1, HSV-1, HSV-2, and PRV gDs with nectin-1, respectively (table S2).

Basis of nectin-1 recognition by BHV-1 gD

We then performed a detailed characterization of the amino acid interactions between the receptor and BHV-1 gD. Along the binding interface, a total of 22 amino acids in BHV-1 gD (table S3) and 21 residues in BO-nectin-1 (table S4) are located within a distance of 4.5 Å of the interaction interface to provide intermolecular contacts. In the N-terminal loop of BHV-1 gD, residues P15 to P18 and W28 to H29 are in close vicinity of the receptor FC and C′C″ strands, respectively (Fig. 4, A and B). Residues P15 to P18 contact nectin-1 residues F129 to P130 and the apolar carbon atoms in the side chain of K61 for hydrophobic interactions (Fig. 4, A and B). Residues W28 to H29 mainly interact with amino acids I80, N82, and M85 to S88 in the receptor, providing both H-bond (BHV-1 gD H29 with nectin-1 G86) and van der Waals (vdw) interactions (Fig. 4, A and B). In contrast to the N-elements that contribute only a limited number of intermolecular contacts, the extension elements at the gD C terminus interacted with the receptor in a much more extensive manner. A large number of residues residing in helices α3, α3′ strand str3, and the G/α2 interloop of the BHV-1 gD were observed to recognize the receptor (Fig. 4A). These included residues Y190, A194, L209 to Y216, A220, A223, I224, and Y227 (Fig. 4C). Reciprocally, the footprint of these gD C-elements in BO-nectin-1 is composed of amino acids T63, Q64, G73 to N77, I80, S88, L90, A127 to P130, and N133, which are interspersed over the whole CC′C″ FG sheet surface. These identified interface residues form an extensive interaction network, providing approximately 63% of the total intermolecular contacts (table S3). In addition, five interchain H-bonds (gD L209 with nectin-1 N77, gD T210 with nectin-1 N77, gD L212 with nectin-1 N77, gD Q214 with nectin-1 Q64, and gD Y216 with nectin-1 T63, respectively) were observed to form, further clinching BHV-1 gD to the nectin-1 receptor (Fig. 4, A and C).

Overall, BHV-1 gD uses a series of residues quite different from those in HSV and PRV gDs for nectin-1 recognition (Fig. 2F), which is in line with the low sequence identity for these viral gDs. As to the nectin-1 receptor, however, essentially the same surface patch in the CC′C″ FG sheet was selected to interface with the gD molecule. Of those identified gD-binding residues (22 residues with HSV-1 gD, 26 with HSV-2 gD, 31 with PRV gD, and 21 with BHV-1 gD), 17 amino acids are shared to engage all gD ligands (table S4). It is also notable that all the residues interfacing with BHV-1 gD are absolutely conserved between BO- and HU-nectin-1 (Fig. 4D), which

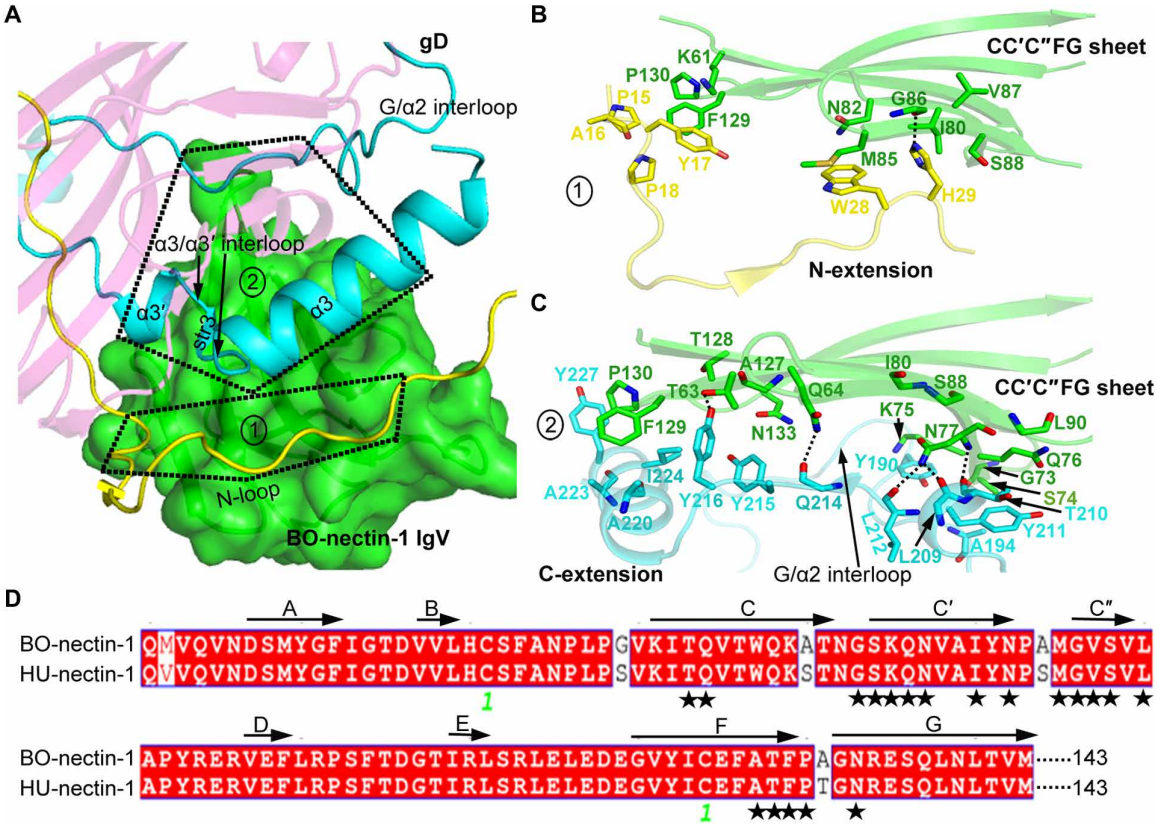

Fig. 4. The atomic interaction details at the BHV-1-gD/BO-nectin-1 interface. (**A**) An overview of the binding interface. The nectin-1 receptor and the gD ligand are shown in surface and cartoon representations, respectively. The interface components in BHV-1 gD, including the N-loop and the multiple elements in the C-terminal extension, are highlighted and marked with patch numbers 1 and 2. The amino acid interaction details for each patch are further delineated in (**B**) and (C), respectively. (**B**) The interaction of gD N-loop with nectin-1. (**C**) The interaction of the gD C-extension elements with nectin-1. For clarity, only those residues providing ≥2 vdw contacts are shown and labeled. A full list of the interface residues are summarized in tables S3 and S4. Dashed lines indicate H-bonds. (**D**) Sequence alignment for the IgV domain of BO-nectin-1 and HU-nectin-1. The residues interfacing with BHV-1 gD are marked with black stars.

explains the similar affinities observed with BHV-1 gD to interact with both the bovine and human receptors.

Arg[188] is a critical residue determining the low-affinity interaction between BHV-1 gD and nectin-1

BHV-1 gD shows a similar nectin-1 binding mode and buries a comparable surface area when compared with other alphaherpesviral gD–nectin-1 interactions; thus, this observation does not explain its low-affinity interaction with nectin-1. We therefore undertook a detailed structural comparison to identify potential molecular features underlying this lower nectin-1 binding affinity. We noted that superimposition of the free and the receptor-bound gD structures revealed a marked conformational difference for the central region of the G/α2 interloop in BHV-1 gD. We therefore first scrutinized the electron density maps of the two structures, paying particular attention to this loop region. As expected, clear and unambiguous densities were observed (fig. S2, A and B), which confirmed the observed differences in conformation before and after receptor binding. In the free gD structure, this loop stretched out toward a neighboring gD molecule related by a twofold symmetry axis (fig. S3). Such a packing mode enabled π-π interactions mediated by two Y190 residues and the formation of H-bonds between R188 and S127 (fig. S3), which, in turn, stabilized the "stretched" conformation for the loop. Upon nectin-1 binding, this interloop changed into a "tilted" conformation. A loop-residing arginine residue (R188) shifted by about 6.8 Å, tilting away from the bound receptor (Fig. 5A). These changes subsequently created sufficient space for nectin-1 engagement, which would otherwise cause strong steric hindrance with nectin-1 amino acids I123 and Q137. In addition, Y190 further rotated its side chain by about 90° along the conformational change in the interloop (Fig. 5A). Overall, R188 does not provide any intermolecular contacts in the complex structure, whereas Y190 interacts with residues G73, S74, and K75 in the receptor via multiple vdw contacts (table S3).

In light of these structural observations, we mutated these two residues to glycine individually in BHV-1 gD and measured real-time binding kinetics between the gD mutants and BO-nectin-1 IgV by SPR. The affinities were determined to be 70.54 ± 13.52 nM for the R188G mutant and 750.2 ± 164.8 nM for the Y190G mutant (Fig. 5, B and C, and Table 1). The affinity of the R188G mutant is about fivefold higher when compared with that of the wild-type gD, which is consistent with the large side chain of R188 interfering with the nectin-1 interaction. The Y190G mutation caused an about twofold decrease in receptor binding affinity, which is in agreement with the observed intermolecular vdw contacts contributed by Y190. The results therefore demonstrated that the G/α2 interloop disturbs nectin-1 binding via the loop-residing R188 residue, which is a critical amino acid determining the low-affinity interaction of BHV-1 gD with the receptor.

We also scrutinized the HSV and PRV gD structures for any nectin-1 binding–induced conformational changes in the equivalent G/α2 interloops. For both HSV-1 and HSV-2 gDs, this interloop is three residues shorter between the two conserved cysteine residues C189 and C202 when compared with that of BHV-1 gD (Fig. 2F) and adopts the same conformation after nectin-1 engagement (Fig. 5D). For PRV gD, its G/α2 interloop is of the same length between C172 and C188 when compared with that of BHV-1 gD (Fig. 2F). However, an α2′ helix forms in the corresponding region, tilting the interloop away from the bound nectin-1 molecule. Accordingly, no obvious conformational change was observed upon receptor binding (Fig. 5E).

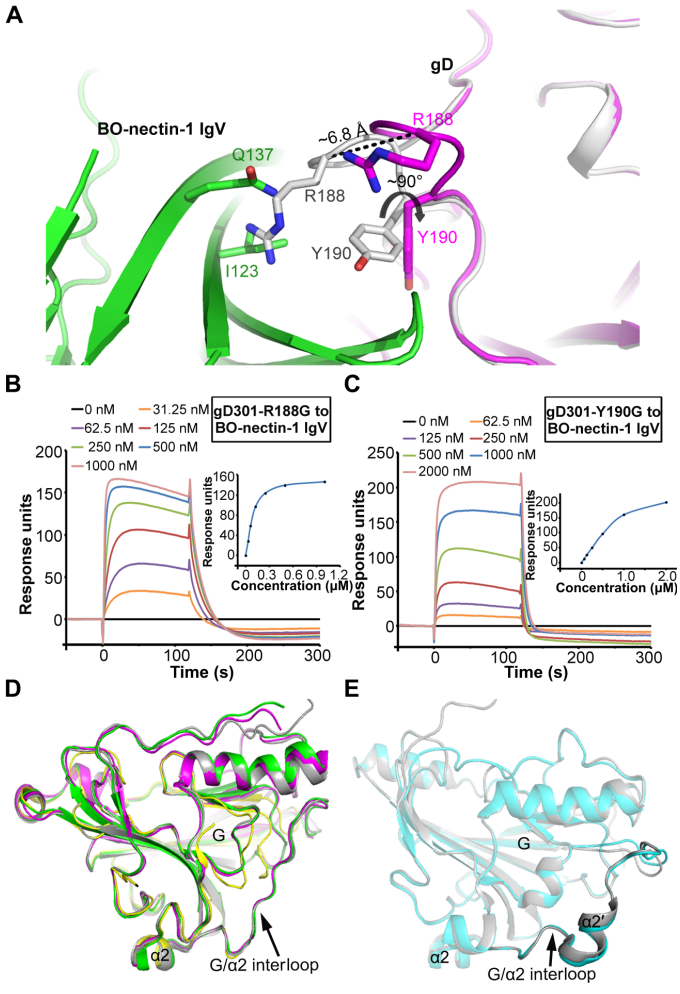

Fig. 5. R188 in the G/α2 interloop interferes with nectin-1 engagement. (**A**) A magnified view on the G/α2 interloop in the free gD structure (gray) and in the nectin-1–bound complex structure (magenta). The nectin-1 receptor is colored green. The residues referred to in the text are shown and labeled. The approximate 6.8-Å shift observed with R188 and about 90° rotation with Y190 are highlighted. (**B** and **C**) SPR experiments characterizing the binding of gD R188G (B) and Y190G (C) mutants to BO-nectin-1 IgV. The representative kinetic profiles are shown. (**D**) Structural comparison of HSV-1 gD in the free (gray) and nectin-1–bound forms (magenta) and of HSV-2 gD in the free (yellow) and nectin-1–bound forms (green). (**E**) Structural comparison of PRV gD in the free (gray) and nectin-1–bound forms (cyan).

DISCUSSION

Consistent with other enveloped viruses, alphaherpesviruses exert their survival strategy by initially interacting with a host cellular receptor(s) (*5*). Although multiple envelope proteins in alphaherpesviruses are required to mediate virus entry, the gD-receptor interaction is a critical step. Nectin-1 serves as the primary receptor used by multiple herpesviruses for entry, including HSV, PRV, and BHV-1 (*12*). Structural data of the full-length extracellular domain of HSV-1 gD reveal that its C terminus is fixed near the N-terminal extension via the PxxW motif (*25*), masking the nectin-1 binding site (*22*, *25*). Thus, the C-terminal loop harboring this motif interferes with the gD/nectin-1 interaction. Consistently, the full ectodomain protein of HSV-1 gD shows about 80-fold lower affinity toward nectin-1 than truncated gD variants and such an affinity difference mainly arises from the decrease in the association rate (*26*). A similar decrease in

k_{on} when interacting with nectin-1 was also reported for PRV gD when a long gD form was compared with the results of a short gD variant (*19*). Notably, BHV-1 gD also has a PxxW motif at the C terminus of its extracellular domain (Fig. 2F). In this report, we have studied the nectin-1 binding kinetics for three BHV-1 gD forms: gD342, which contains the PxxW motif, and gD301 and gD274 that lack this motif. Although their accurate k_{on} rates were not determined (gD342 shows slow-on/fast-off kinetics for which no accurate algorithm model is available, and gD301 and gD274 both show a fast-on/fast-off mode with which the steady-state affinity model does not quantitatively calculate the k_{on} and k_{off} rates), the observed kinetic change (from a fast-on binding for gD301 and gD274 to a slow-on binding for gD342) also features an obvious decrease in the association rate. We therefore postulate that the PxxW motif at the BHV-1 gD C terminus also likely pre-locks the nectin-1 binding site as observed in HSV. The engagement of the receptor should subsequently displace the C-terminal loop, echoing the C-terminal displacement in HSV gD that is proposed to switch on its prefusion domain (PFD) to activate the fusion executor composed of gB, gH, and gL (*25*).

Although it has long been observed that BHV-1 gD interacts with lower affinity to nectin-1 when compared with that of other alphaherpesviral gDs (*12*), this reduced affinity has not been characterized in detail previously. Using the truncated forms of BHV-1 gD, we are able to calculate the binding affinities between the BHV-1 ligand and the nectin-1 receptor. In comparison to that of HSV and PRV gDs (*19*, *21*, *22*, *26*), the determined K_D value for BHV-1 gD highlights more than a 20-fold lower affinity toward nectin-1. Despite the significant difference in affinity, our structures show that BHV-1 gD engages the nectin-1 receptor in a similar manner to that of HSV and PRV gDs. In addition, BHV-1 gD buries an essentially comparable surface area at the binding interface when compared with the surface areas buried for the HSV and PRV gD–nectin-1 interactions. Because crystallization normally traps a protein or a protein complex in the lowest energy state (in which the protein/protein complex is likely the most stable), we believe that the solved complex structures should have captured the viral ligand interacting with its receptor at the final bound stage. In such a context, it is expected that HSV, PRV, and BHV-1 gDs, while exhibiting similar nectin-1 binding modes, bury comparable surface areas in the receptor in their complex structures. The lower binding affinity for the nectin-1–BHV-1-gD interaction should, therefore, be related to elements featured during the interaction process. Our structures reveal that the G/α2 interloop experiences a large conformational change upon nectin-1 binding, tilting away residue R188 in the interloop to create sufficient space for receptor binding. The stretched conformation observed in the free structure was stabilized by a neighboring molecule, which raises the possibility that it might be the result of packing artifacts. However, this is unlikely the case because mutation of R188 to glycine increased the binding affinity of BHV-1 gD to nectin-1 by about fivefold, which is in agreement with our observations that R188 would otherwise cause strong steric clashes with nectin-1. These results demonstrate that the BHV-1 G/α2 interloop interferes with nectin-1 binding, and changes from a stretched to a tilted conformation represent a prerequisite for receptor engagement.

Notably, such a conformational change in the G/α2 interloop is not observed in HSV and PRV gDs. The gD of HSV contains a loop that is three residues shorter than that of BHV-1 gD. Thus, the HSV interloop is postulated to be too short to interfere with nectin-1 binding. The gD of PRV has a G/α2 interloop of similar size to the BHV-1 protein. An α2′ helix, however, forms in the equivalent loop region, causing the interloop to tilt away and thus does not interfere with receptor binding. These observations highlight a divergent evolution process for alphaherpesviruses during which the nectin-1 engagement mode by gDs is essentially preserved, but virus-specific features have evolved to modulate their receptor binding affinities.

Nectin-1 can regulate a series of cellular activities such as cell polarization, differentiation, movement, and proliferation (*14*). Previous studies have found that nectin-1 is expressed highly in cancer-associated fibroblasts and pancreatic ductal adenocarcinoma cells (*15*, *16*). Notably, the abundance of nectin-1 on the cell surface is proposed to render cells susceptible to herpesviruses infection (*6*). Furthermore, the nectin-1 level in squamous cell carcinoma has been shown to correlate strongly with herpesviral oncolysis (*24*). It is interesting that the R188G mutation in BHV-1 gD could enhance its binding affinity to nectin-1. We find that improved binding of gD to nectin-1 does not necessarily correlate with increased efficiencies of virus infection. Certain affinity-enhancing mutations in HSV-1 gD could result in viruses that are impaired in infection (*27*, *28*). For these gD mutants, however, the mutations are commonly located in the functional regions of gD that could affect virus fusion. For instance, deletion of residues 290 to 299 in HSV-1 gD could significantly increase its binding affinity to nectin-1, but the virus bearing the deletion is of lower infection efficiency than the wild-type virus (*27*). We find that the deleted region in HSV-1 gD contains the PxxW motif. Residues P291 and W294 in the motif could contact the N-terminal extension region and help anchor the protein C terminus to the proximity of the N terminus (*25*). Such a "pre-locked" C-terminal loop could enable concerted displacement of the loop upon nectin-1 binding, thereby exposing PFD to activate membrane fusion (*29*, *30*). The deletion of the motif (and/or any mutations impairing the C-loop displacement) could likely impair the fusion process, resulting into decreased virus infection despite that the capacity of gD binding to nectin-1 is enhanced. Conversely, when this characteristic "pre-locked C-loop" is reserved, enhanced receptor engagement by gD seems to lead to increased virus infection. As a representative example of such mutations (*31*), the Q27P substitution in HSV-1 gD is shown to enhance the binding capacity of gD to nectin-1 by about 2.5-fold. Accordingly, the infection efficiency of the virus containing gD-Q27P is observed to be about 1.3-fold higher than that of the wild-type virus. In our structure, residue R188 is sterically far away from the PxxW-accommodating site (fig. S4) and is therefore unlikely affecting the C-loop interaction with the main body of BHV-1 gD. In such a context, BHV-1 virus bearing gD-R188G mutation might exhibit enhanced infection capability. In light of multiple previous studies reporting the potential use of BHV-1 for oncolysis (*4*, *32*), we believe that examining the oncolytic effect of a BHV-1 variant containing the gD-R188G mutation represents a worthy future endeavor.

MATERIALS AND METHODS

Protein expression and purification

The IgV domain proteins of bovine (BO-nectin-1) and human (HU-nectin-1) were prepared with the prokaryotic expression system following the reported methods (*22*). Briefly, the coding fragments for BO-nectin-1 residues 37 to 145 and HU-nectin-1 residues 37 to 145 were individually cloned in to the pET-21a (Invitrogen) vector with the Nde I and Eco RI restriction sites and subsequently

transformed into *Escherichia coli* BL21(DE3) for protein expression. The proteins were expressed as inclusion bodies, which are extracted first with the buffer consisting of 0.5% Triton X-100, 50 mM tris-HCl (pH 8.0), 300 mM NaCl, 10 mM EDTA, and 10 mM dithiothreitol (DTT) and then with the buffer of 50 mM tris-HCl (pH 8.0), 100 mM NaCl, 10 mM EDTA, and 10 mM DTT. The inclusion bodies were then dissolved in a buffer consisting of 6 M guanidine hydrochloride, 10% glycerol, 50 mM tris-HCl (pH 8.0), 100 mM NaCl, 10 mM EDTA, and 10 mM DTT. For protein refolding, the dissolved inclusion bodies were dropwise diluted into a buffer composed of 100 mM tris-HCl (pH 9.0), 400 mM L-arginine, 2 mM EDTA, 5 mM reduced glutathione, and 0.5 mM oxidized glutathione and then incubated overnight to complete the refolding process. The refolded proteins were then concentrated using a 5-kDa cutoff membrane with an Amicon Stirred Cell concentrator (Merck Millipore) and then exchanged into a buffer consisting of 20 mM tris-HCl (pH 8.0), 500 mM NaCl, 10% glycerol, and 1 mM DTT. Subsequently, the proteins were further purified by gel filtration with a Superdex 200 increase 10/300 GL (GE Healthcare) column.

The ectodomain proteins (wild type and mutants) of BHV-1 gD were prepared in insect cells using the Bac-to-Bac baculovirus expression system (Invitrogen). Briefly, the DNA fragments coding for BHV-1 (strain P8-2) gD residues 1 to 274 (gD274), 1 to 301 (gD301), and 1 to 342 (gD342), as well as the coding fragments for the R188G- and Y190G-gD301 mutants, were first amplified to include a C-terminal 6× his coding sequence and then individually subcloned, via the Eco RI and Xho I sites, into a previously modified pFast-Bac1 vector, which had been engineered to incorporate a baculovirus gp67 signal sequence at the N terminus (*22*). Transfection and virus amplification were then conducted with Sf9 cells, and the recombinant proteins were produced in Hi5 cells. For primary protein purification, the culture supernatant containing the target proteins was passed through a 5-ml HisTrap excel column (GE Healthcare) for affinity chromatography. The eluted protein was further purified by ion exchange with a Source 15Q column (GE Healthcare) and then by gel filtration using a Superdex 200 Increase 10/300 GL column (GE Healthcare). All the proteins were lastly exchanged into a buffer consisting of 20 mM tris-HCl (pH 8.0) and 150 mM NaCl for further use.

Analytical gel filtration chromatography

Purified BO-/HU-nectin-1 IgV and gD301 were individually mixed at a molar ratio of 3:1 in advance. The subsequent protein mixtures were then incubated on ice for ~4 hours and then loaded onto a calibrated Superdex 200 Increase 10/300 GL (GE Healthcare) column for analysis. The single gD301 and BO-/HU-nectin-1 IgV-domain proteins were analyzed with the same column and the chromatographs were superimposed for comparison. The pooled samples were further analyzed by SDS–polyacrylamide gel electrophoresis (15% gel) and stained with Coomassie blue.

SPR measurements

The binding affinities between the indicated gD proteins (wild type and mutants) and the BO-/HU-nectin-1 were analyzed at 25°C on a Biacore X-100 machine with the nitrilotriacetic acid chips (GE Healthcare). The running buffer contains 10 mM Hepes (pH 7.4), 150 mM NaCl, and 0.005% Tween 20. About 600 response units of the gD proteins (containing a C-terminal 6× his tag) were immobilized on chips, and the blank channel was used as the negative control. A serial of two-fold diluted nectin-1 IgV were flowed over the gD protein for kinetic determination. In each binding cycle, the sensor surface was regenerated with 350 mM EDTA and then with 0.5 mM $NiCl_2$. The obtained kinetic data of gD301 and gD274 binding to nectin-1 were then analyzed with the BIAevaluation software 4.1 using the steady-state affinity model. For the binding data between gD342 and nectin-1, the affinity values were not calculated because no accurate fitting algorithms are applicable. For each binding pair, three independent kinetic assays were conducted, and the calculated kinetic parameters are summarized in Table 1.

Crystallization

The free BHV-1 gD protein and the gD/BO-nectin-1-IgV complex were crystallized by the sitting-drop vapor diffusion method. The initial crystallization screening was conducted with the commercial Hampton Research and Molecular Dimensions kits, and those conditions support crystal growth were further optimized. The free BHV-1 gD crystals were lastly obtained by mixing 1 μl of the concentrated gD301 protein at 10 mg/ml with 1 μl of reservoir solution consisting of 0.2 M ammonium acetate, 0.1 M tris-HCl (pH 8.0), and 16% (w/v) polyethylene glycol 10,000, followed by incubation at 18°C for about 1 week. To obtain crystals for the BHV-1-gD/BO-nectin-1-IgV complex, purified gD301 and BO-nectin-1 IgV were initially mixed at 1:3 molar ratio and incubated on ice for ~4 hours. The mixture was further purified by gel filtration chromatography using a Superdex 200 increase 10/300 GL (GE Healthcare) column. The protein complex was then collected and concentrated to 10 mg/ml. Diffractable crystals were lastly obtained by mixing 1 μl of the protein complex with 1 μl of reservoir solution consisting of 0.1 M sodium Hepes (pH 7.0) and 15% (w/v) polyethylene glycol 4000, followed by incubation at 8°C for about 1 month.

Data collection and structure determination

For crystal preparation, all crystals were cryo-protected by sequentially soaking the crystals first in a cryo-protectant composed of 10% (v/v) glycerol and 90% (v/v) reservoir solution and then in a cryo-protectant with 20% (v/v) glycerol and 80% (v/v) reservoir solution, followed by flash-cooling in liquid nitrogen. Diffraction data were then collected at beamline BL19U1 (*33*) of the Shanghai Synchrotron Radiation Facility using the synchrotron radiation at 100 K. The collected data were processed with HKL2000 (*34*) for indexing, integration, and scaling. The structures of the free BHV-1 gD and the BHV-1-gD/BO-nectin-1-IgV complex were solved by molecular replacement with Phaser (*35*) in CCP4 (*36*) using the free PRV gD structure [Protein Data Bank (PDB) code 5X5V] and the PRV-gD/nectin-1-IgV complex structure (PDB code 5X5W) as the search models, respectively. The atomic models were completed with Coot (*34*), refined with REFMAC (*37*), followed by rounds of manual adjustment in Coot (*38*). Further structural refinement was carried out with Phenix (*39*). The stereochemical qualities of the final models were assessed with PROCHECK (*40*). The final data processing and structure refinement statistics are summarized in table S1. All structural figures were generated using PyMOL (www.pymol.org).

SUPPLEMENTARY MATERIALS

Supplementary material for this article is available at http://advances.sciencemag.org/cgi/content/full/6/20/eaba5147/DC1

View/request a protocol for this paper from *Bio-protocol*.

REFERENCES AND NOTES

1. C. Jones, S. Chowdhury, A review of the biology of bovine herpesvirus type 1 (BHV-1), its role as a cofactor in the bovine respiratory disease complex and development of improved vaccines. *Anim. Health Res. Rev.* **8**, 187–205 (2007).
2. R. Rodrigues, B. Cuddington, K. Mossman, Bovine herpesvirus type 1 as a novel oncolytic virus. *Cancer Gene Ther.* **17**, 344–355 (2010).
3. B. P. Cuddington, K. L. Mossman, Permissiveness of human cancer cells to oncolytic bovine herpesvirus 1 is mediated in part by KRAS activity. *J. Virol.* **88**, 6885–6895 (2014).
4. B. P. Cuddington, K. L. Mossman, Oncolytic bovine herpesvirus type 1 as a broad spectrum cancer therapeutic. *Curr. Opin. Virol.* **13**, 11–16 (2015).
5. R. J. Eisenberg, D. Atanasiu, T. M. Cairns, J. R. Gallagher, C. Krummenacher, G. H. Cohen, Herpes virus fusion and entry: A story with many characters. *Viruses* **4**, 800–832 (2012).
6. P. G. Spear, R. Longnecker, Herpesvirus entry: An update. *J. Virol.* **77**, 10179–10185 (2003).
7. S. Manoj, C. R. Jogger, D. Myscofski, M. Yoon, P. G. Spear, Mutations in herpes simplex virus glycoprotein D that prevent cell entry via nectins and alter cell tropism. *Proc. Natl. Acad. Sci. U.S.A.* **101**, 12414–12421 (2004).
8. V. Tiwari, C. Clement, D. Xu, T. Valyi-Nagy, B. Y. Yue, J. Liu, D. Shukla, Role for 3-O-sulfated heparan sulfate as the receptor for herpes simplex virus type 1 entry into primary human corneal fibroblasts. *J. Virol.* **80**, 8970–8980 (2006).
9. R. I. Montgomery, M. S. Warner, B. J. Lum, P. G. Spear, Herpes simplex virus-1 entry into cells mediated by a novel member of the TNF/NGF receptor family. *Cell* **87**, 427–436 (1996).
10. R. J. Geraghty, C. Krummenacher, G. H. Cohen, R. J. Eisenberg, P. G. Spear, Entry of alphaherpesviruses mediated by poliovirus receptor-related protein 1 and poliovirus receptor. *Science* **280**, 1618–1620 (1998).
11. P. G. Spear, R. J. Eisenberg, G. H. Cohen, Three classes of cell surface receptors for alphaherpesvirus entry. *Virology* **275**, 1–8 (2000).
12. S. A. Connolly, J. J. Whitbeck, A. H. Rux, C. Krummenacher, S. van Drunen Littel-van den Hurk, G. H. Cohen, R. J. Eisenberg, Glycoprotein D homologs in herpes simplex virus type 1, pseudorabies virus, and bovine herpes virus type 1 bind directly to human HveC (nectin-1) with different affinities. *Virology* **280**, 7–18 (2001).
13. K. Mandai, Y. Rikitake, M. Mori, Y. Takai, Nectins and nectin-like molecules in development and disease. *Curr. Top. Dev. Biol.* **112**, 197–231 (2015).
14. H. Ogita, Y. Takai, Nectins and nectin-like molecules: Roles in cell adhesion, polarization, movement, and proliferation. *IUBMB Life* **58**, 334–343 (2006).
15. M. Yamada, K. Hirabayashi, A. Kawanishi, A. Hadano, Y. Takanashi, H. Izumi, Y. Kawaguchi, T. Mine, N. Nakamura, T. Nakagohri, Nectin-1 expression in cancer-associated fibroblasts is a predictor of poor prognosis for pancreatic ductal adenocarcinoma. *Surg. Today* **48**, 510–516 (2018).
16. A. Tampakis, E. C. Tampaki, A. Nonni, R. Droeser, A. Posabella, G. Tsourouflis, K. Kontzoglou, E. Patsouris, M. von Flüe, G. Kouraklis, Nectin-1 expression in colorectal cancer: Is there a group of patients with high risk for early disease recurrence? *Oncology* **96**, 318–325 (2019).
17. D. Samanta, S. C. Almo, Nectin family of cell-adhesion molecules: Structural and molecular aspects of function and specificity. *Cell. Mol. Life Sci.* **72**, 645–658 (2015).
18. E. Ono, Y. Tomioka, Y. Watanabe, K. Amagai, S. Taharaguchi, J. Glenisson, P. Cherel, The first immunoglobulin-like domain of porcine nectin-1 is sufficient to confer resistance to pseudorabies virus infection in transgenic mice. *Arch. Virol.* **151**, 1827–1839 (2006).
19. A. Li, G. Lu, J. Qi, L. Wu, K. Tian, T. Luo, Y. Shi, J. Yan, G. F. Gao, Structural basis of nectin-1 recognition by pseudorabies virus glycoprotein D. *PLOS Pathog.* **13**, e1006314 (2017).
20. P. Di Giovine, E. C. Settembre, A. K. Bhargava, M. A. Luftig, H. Lou, G. H. Cohen, R. J. Eisenberg, C. Krummenacher, A. Carfi, Structure of herpes simplex virus glycoprotein D bound to the human receptor nectin-1. *PLOS Pathog.* **7**, e1002277 (2011).
21. G. Lu, N. Zhang, J. Qi, Y. Li, Z. Chen, C. Zheng, G. F. Gao, J. Yan, Crystal structure of herpes simplex virus 2 gD bound to nectin-1 reveals a conserved mode of receptor recognition. *J. Virol.* **88**, 13678–13688 (2014).
22. N. Zhang, J. Yan, G. Lu, Z. Guo, Z. Fan, J. Wang, Y. Shi, J. Qi, G. F. Gao, Binding of herpes simplex virus glycoprotein D to nectin-1 exploits host cell adhesion. *Nat. Commun.* **2**, 577 (2011).
23. R. M. Johnson, P. G. Spear, Herpes simplex virus glycoprotein D mediates interference with herpes simplex virus infection. *J. Virol.* **63**, 819–827 (1989).
24. Z. Yu, P. S. Adusumilli, D. P. Eisenberg, E. Darr, R. A. Ghossein, S. Li, S. Liu, B. Singh, J. P. Shah, Y. Fong, R. J. Wong, Nectin-1 expression by squamous cell carcinoma is a predictor of herpes oncolytic sensitivity. *Mol. Ther.* **15**, 103–113 (2007).
25. C. Krummenacher, V. M. Supekar, J. C. Whitbeck, E. Lazear, S. A. Connolly, R. J. Eisenberg, G. H. Cohen, D. C. Wiley, A. Carfi, Structure of unliganded HSV gD reveals a mechanism for receptor-mediated activation of virus entry. *EMBO J.* **24**, 4144–4153 (2005).
26. C. Krummenacher, A. H. Rux, J. C. Whitbeck, M. Ponce-de-Leon, H. Lou, I. Baribaud, W. F. Hou, C. H. Zou, R. J. Geraghty, P. G. Spear, R. J. Eisenberg, G. H. Cohen, The first immunoglobulin-like domain of HveC is sufficient to bind herpes simplex virus gD with full affinity, while the third domain is involved in oligomerization of HveC. *J. Virol.* **73**, 8127–8137 (1999).
27. R. S. B. Milne, S. L. Hanna, A. H. Rux, S. H. Willis, G. H. Cohen, R. J. Eisenberg, Function of herpes simplex virus type 1 gD mutants with different receptor-binding affinities in virus entry and fusion. *J. Virol.* **77**, 8962–8972 (2003).
28. H. Y. Chiang, G. H. Cohen, R. J. Eisenberg, Identification of functional regions of herpes simplex virus glycoprotein gD by using linker-insertion mutagenesis. *J. Virol.* **68**, 2529–2543 (1994).
29. F. Cocchi, D. Fusco, L. Menotti, T. Gianni, R. J. Eisenberg, G. H. Cohen, G. Campadelli-Fiume, The soluble ectodomain of herpes simplex virus gD contains a membrane-proximal pro-fusion domain and suffices to mediate virus entry. *Proc. Natl. Acad. Sci. U.S.A.* **101**, 7445–7450 (2004).
30. D. Fusco, C. Forghieri, G. Campadelli-Fiume, The pro-fusion domain of herpes simplex virus glycoprotein D (gD) interacts with the gD N terminus and is displaced by soluble forms of viral receptors. *Proc. Natl. Acad. Sci. U.S.A.* **102**, 9323–9328 (2005).
31. S. A. Connolly, D. J. Landsburg, A. Carfi, J. C. Whitbeck, Y. Zuo, D. C. Wiley, G. H. Cohen, R. J. Eisenberg, Potential nectin-1 binding site on herpes simplex virus glycoprotein D. *J. Virol.* **79**, 1282–1295 (2005).
32. L. Zhu, X. Fu, C. Yuan, X. Jiang, G. Zhang, Induction of oxidative DNA damage in bovine herpesvirus 1 infected bovine kidney cells (MDBK Cells) and human tumor cells (A549 Cells and U2OS Cells). *Viruses* **10**, E393 (2018).
33. W.-Z. Zhang, J.-C. Tang, S.-S. Wang, Z.-J. Wang, W.-M. Qin, J.-H. He, The protein complex crystallography beamline (BL19U1) at the Shanghai Synchrotron radiation facility. *Nucl. Sci. Tech.* **30**, 170 (2019).
34. Z. Otwinowski, W. Minor, [20] Processing of X-ray diffraction data collected in oscillation mode. *Methods Enzymol.* **276**, 307–326 (1997).
35. R. J. Read, Pushing the boundaries of molecular replacement with maximum likelihood. *Acta Crystallogr. D Biol. Crystallogr.* **57**, 1373–1382 (2001).
36. Collaborative Computational Project, Number 4, The CCP4 suite: Programs for protein crystallography. *Acta Crystallogr. D Biol. Crystallogr.* **50**, 760–763 (1994).
37. G. N. Murshudov, A. A. Vagin, E. J. Dodson, Refinement of macromolecular structures by the maximum-likelihood method. *Acta Crystallogr. D Biol. Crystallogr.* **53**, 240–255 (1997).
38. P. Emsley, K. Cowtan, Coot: Model-building tools for molecular graphics. *Acta Crystallogr. D Biol. Crystallogr.* **60**, 2126–2132 (2004).
39. T. C. Terwilliger, R. W. Grosse-Kunstleve, P. V. Afonine, N. W. Moriarty, P. H. Zwart, L.-W. Hung, R. J. Read, P. D. Adams, Iterative model building, structure refinement and density modification with the *PHENIX AutoBuild* wizard. *Acta Crystallogr. D Biol. Crystallogr.* **64**, 61–69 (2008).
40. R. A. Laskowski, J. A. C. Rullmann, M. W. MacArthur, R. Kaptein, J. M. Thornton, AQUA and PROCHECK-NMR: Programs for checking the quality of protein structures solved by NMR. *J. Biomol. NMR* **8**, 477–486 (1996).

Acknowledgments: We thank the staff of BL19U1 beamline at National Center for Protein Sciences Shanghai and Shanghai Synchrotron Radiation Facility (Shanghai, People's Republic of China) for assistance during data collection. We also thank Liwen Bianji, Edanz Editing China (www.liwenbianji.cn/ac) for editing the English text. **Funding:** This work was supported by the National Natural Science Foundation of China (grant nos. 81971925 and 31570157), the National International Science and Technology Cooperation Project (grant no. 2015DFA30690), the National Key R&D Program of China (grant no. 2016YFC1200305), and the Outstanding Youth Foundation of Sichuan University (grant no. 2016SCU04B01). **Author contributions:** G.L. and Y.L. conceived the study. G.L. and Zhujun Chen supervised the whole project. D.Y. performed the experiments and analysis. F.Ye., F.Ya., and S.L. collected the datasets and G.L. solved the structures. Y.Ch., J.W., Zimin Chen, X.L., J.Y., H.C., Z.Z., Y.Y., H.S., A.W., L.W., and Y.Z. assisted with the cell maintenance and protein preparations. G.L. and D.Y. wrote the manuscript, and B.H. and Y.Ca. participated in the manuscript editing and discussion. **Competing interests:** The authors declare that they have no competing interests. **Data and materials availability:** All data needed to evaluate the conclusions in the paper are present in the paper and/or the Supplementary Materials. Additional data related to this paper may be requested from the authors. Coordinates and structure factors are deposited in the PDB with ID nos. 6LS9 and 6LSA.

Submitted 10 December 2019
Accepted 28 February 2020
Published 13 May 2020
10.1126/sciadv.aba5147

Citation: D. Yue, Z. Chen, F. Yang, F. Ye, S. Lin, B. He, Y. Cheng, J. Wang, Z. Chen, X. Lin, J. Yang, H. Chen, Z. Zhang, Y. You, H. Sun, A. Wen, L. Wang, Y. Zheng, Y. Cao, Y. Li, G. Lu, Crystal structure of bovine herpesvirus 1 glycoprotein D bound to nectin-1 reveals the basis for its low-affinity binding to the receptor. *Sci. Adv.* **6**, eaba5147 (2020).